Some aspects of DM, EWPT, LHC searches and prospects of detecting the gravitational waves in Z_3- NMSSM

Subhojit Roy

Harish-Chandra Research Institute
Allahabad, India

Based on JHEP06(2022)108, arXiv:2202.12476

Online HEP Seminar Series

Indian Institute of Technology,Hyderabad

September 22, 2022

Outline

NMSSM Motivation

Electroweak Phase transition and Baryogenesis and the NMSSM

Viability of SFOEWPT in the NMSSM in view of collider and DM constraints

Gravitational waves from FOEWPT

Conclusion

NMSSM Motivation

Inclusion of a singlet superfield $\widehat{S}$

$\Rightarrow$ an elegant solution to the "μ-problem" of MSSM

Ameliorates the "little hierarchy" problem of MSSM

$\rightarrow$ Can be more "natural" (fine-tuning is small) than MSSM

Richer Higgs and Dark Matter (DM) sectors

More natural set up for SM-like Higgs mass compared to MSSM

Strong first order phase transition for EW baryogenesis may still possible

Singlet Extention of MSSM

singlet extention of MSSM $\longrightarrow$ NMSSM could satisfy SFOEWPT without light squarks due to additional tree-level cubic interaction $\widehat{S}\widehat{H}_u.\widehat{H}_d$ plus thermal loop corrections from the additional singlet-like scalars.

$$\mathcal{W} = \mathcal{W}_{\rm MSSM}|_{\mu=0} + \lambda \widehat{S}\widehat{H}_u.\widehat{H}_d + \frac{\kappa}{3}\widehat{S}^3$$

$$\lambda < S > \widehat{H}_u.\widehat{H}_d \rightarrow \mu_{eff}\widehat{H}_u.\widehat{H}_d$$

Solution to the well-known 'μ' -problem

$$-\mathcal{L}^{\rm soft} = -\mathcal{L}^{\rm soft}_{\rm MSSM}|_{B\mu=0} + m_S^2|S|^2 + (\lambda A_\lambda S H_u \cdot H_d + \frac{\kappa}{3}A_\kappa S^3 + {\rm h.c.}).$$

Additional tree-level cubic terms

Larger trilinear couplings increase the tree-level cubic terms

Pietroni, 9207227

When compared with MSSM, NMSSM have extra one CP-even (h_S) and one CP -odd (a_S) state in the neutral Higgs sector.

Is SFOEWPT in NMSSM still possible?

The scalar (Higgs) sector of NMSSM

Squared mass of the SM-like Higgs boson:

$$m_{h_{SM}}^2 = m_Z^2 \cos^2 2\beta + \lambda^2 v^2 \sin^2 2\beta + \Delta_{\mathrm{mix}} + \Delta_{\mathrm{rad.corr}}$$

Ellwanger et al., Phys.Rept. 496 (2010) 1-77

Extra tree-level correction in NMSSM.

125 GeV Higgs mass without significant radiative corrections at relatively larger λ

Tree level squared mass of singlet-like Higgs states:

$$m_{h_S}^2 = \lambda A_\lambda \frac{v_u v_d}{v_S} + \frac{m_{\tilde{S}}}{2}(A_\kappa + 2m_{\tilde{S}})$$

$$m_{a_S}^2 = \lambda(A_\lambda + 2m_{\tilde{S}})\frac{v_u v_d}{v_S} - \frac{3}{2}A_\kappa m_{\tilde{S}}$$

The electroweakino (ewino) sector

- The symmetric neutralino mass matrix has got a dimensionality of 5×5 and, in the basis $\psi^0 = \{\widetilde{B},\ \widetilde{W}^0,\ \widetilde{H}_d^0,\ \widetilde{H}_u^0,\ \widetilde{S}\}$, is given by

$$\mathcal{M}_0 = \begin{pmatrix} M_1 & 0 & -\frac{g_1 v_d}{\sqrt{2}} & \frac{g_1 v_u}{\sqrt{2}} & 0 \\ & M_2 & \frac{g_2 v_d}{\sqrt{2}} & -\frac{g_2 v_u}{\sqrt{2}} & 0 \\ & & 0 & -\mu_{\rm eff} & -\lambda v_u \\ & & & 0 & -\lambda v_d \\ & & & & 2\kappa v_S \end{pmatrix}$$

$M_1,\ M_2 \rightarrow$ soft SUSY breaking masses for the $U(1)_Y$ and the $SU(2)_L$ gauginos, i.e., the bino and the wino, respectively.

$m_{\widetilde{S}} = 2\kappa v_S = 2\frac{\kappa}{\lambda}\mu_{\rm eff} \rightarrow$ singlino mass term.

New Ewino state of NMSSM “singlino” $\longrightarrow$ a popular CDM candidate

The ewino sector

The neutralino mass-eigenstates (χ_i^0), in terms of the weak eigenstates (ψ_j^0), are given by

$$\chi_i^0 = N_{ij}\psi_j^0$$

'N' is the 5×5 matrix that diagonalizes the neutralino mass-matrix.

The 2×2 chargino mass matrix in the bases $\psi^+ = \{-i\widetilde{W}^+, \widetilde{H}_u^+\}$ and $\psi^- = \{-i\widetilde{W}^-, \widetilde{H}_d^-\}$ is given by

$$\mathcal{M}_C = \begin{pmatrix} M_2 & g_2 v_u \\ g_2 v_d & \mu_{\text{eff}} \end{pmatrix}$$

The asymmetric matrix $\mathcal{M}_C$ can be diagonalized by two 2×2 unitary matrices U and V:

$$U^* \mathcal{M}_C V^\dagger = \text{diag}(m_{\chi_1^\pm}, m_{\chi_2^\pm}) \ ; \quad \text{with} \ \ m_{\chi_1^\pm} < m_{\chi_2^\pm}$$

Requirements for EWBG

Baryon asymmetry parameter $Y_B \equiv \frac{n_B}{s} \sim \frac{1}{7.04}\frac{n_B}{n_\gamma} \sim 10^{-10}$ from Big-bang nucleosynthesis (BBN) and cosmic microwave background (CMB)

Three necessary ingredients needed to create a baryon asymmetry (Sakharov's conditions):

1> B-violation

2> C and CP -violation

3> Departure from Thermal equilibrium

Requirements for EWBG

1> B -violation → Possible from SU(2) sphalerons

2> C and CP -violation → Present in SM but not large enough

3> **Departure from Thermal equilibrium**

→ **Requires Strong FOPT in the Higgs sector**

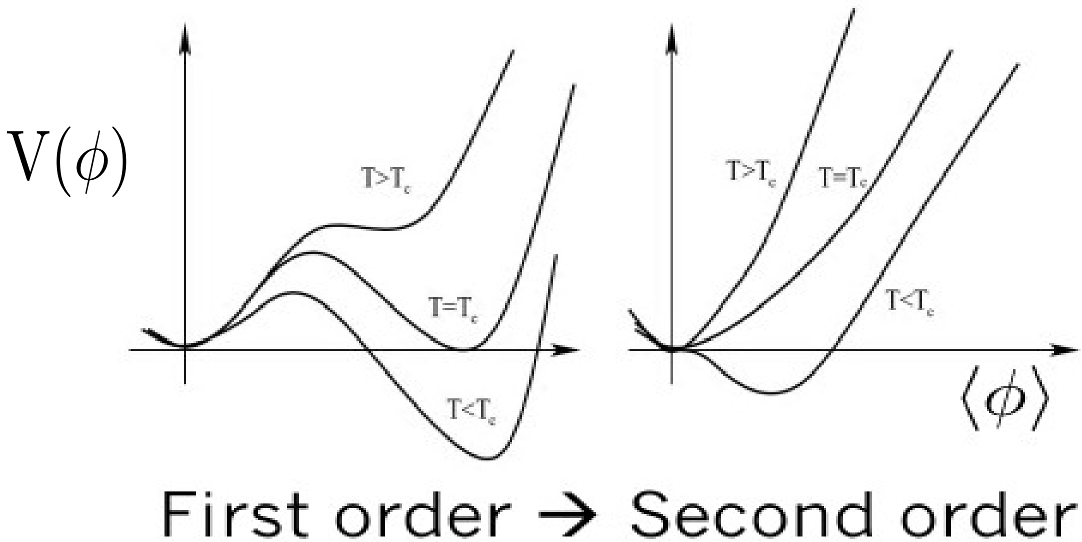

Dine+Kusenko, 0303065

m_h →

← Additional new scalars
(add cubic terms in the potential)

EWBG

Eletroweak baryogenesis (EWBG) refers to a mechanism that creates an asymmetry in the density of baryons during the electroweak phase transition.

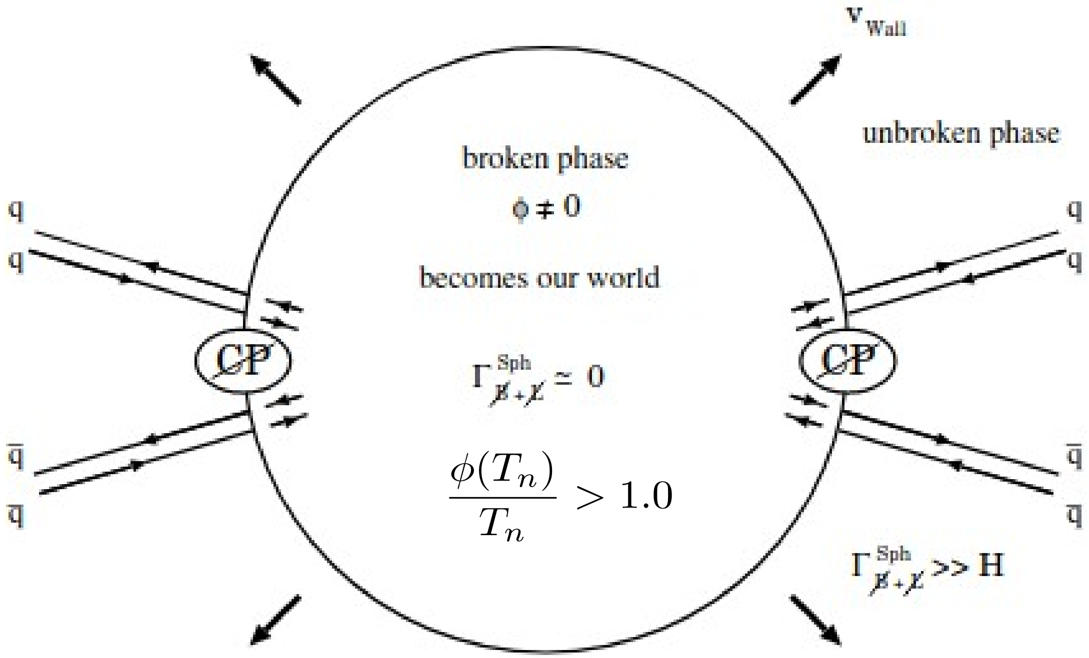

Bernreuther,0205279

EWBG requires Strong FOPT in the SU(2) field directions

$$\gamma_{EW} = \frac{\Delta_{SU(2)}}{T_n} > 1$$

EWPT in Standard Model

For SFOEWPT in standard model (SM) $m_{h_{SM}}$ < 70 ~ 80 GeV

Kajantie, Laine, Rummukainen, Shaposhnikov (1995-98)
Csikor, Fodor, Heitger (1998)

Discovery of 125 GeV Higgs mass rules out FOPT in SM

→ EWBG is not possible in SM

Also CP violation present in the SM but not large enough

→ Need to go beyond SM

New sources of CP-violation and SFOEWPT may arise in supersymmetry.

EWPT in MSSM

SFOPT requires large cubic term in the scalar porential

Bosonic dof add extra cubic terms to the finite temperature effective potential.

$$V_1(T>0) = V_1(T=0) + \frac{T^2}{2\pi^2}\sum_i n_i J_\pm\left(\frac{m_i^2}{T^2}\right)$$

$$J_\pm(x^2) \equiv \pm\int_0^\infty dy\, y^2 \log\left(1 \mp e^{-\sqrt{y^2+x^2}}\right) \xrightarrow[\text{for bosons}]{\text{High-}T\text{ expansion}} \simeq -\frac{\pi^4}{45} + \frac{\pi^2 m^2}{12T^2} - \frac{\pi}{6}\left(\frac{m^2}{T^2}\right)^{3/2} + \cdots$$

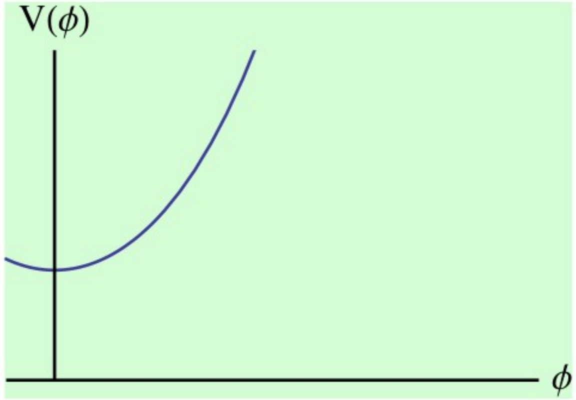

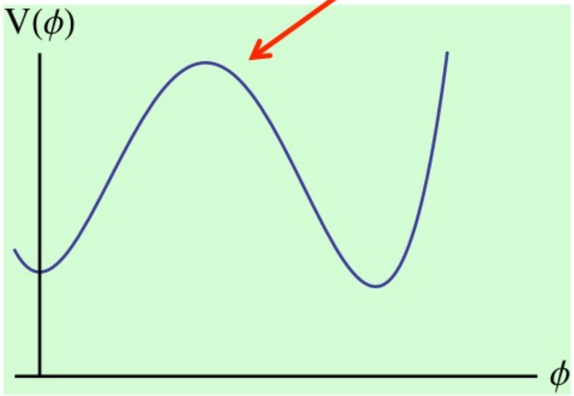

Light top squarks (as bosons add cubic loop contribution) are needed to satisfy SFOEWPT in MSSM.

→ Light stop (below 120 GeV) ruled out from LHC direct searches

→ EWBG in MSSM is not possible now

kozaczuk's slide

Study of the Higgs potential at finite temperature

$$V_{\text{Total}} = V_{\text{Tree}} + V_{\text{CW}}^{\text{1-loop}} + V_{\text{counter terms}} + V_{\text{T}}^{\text{1-loop}} + V_{\text{daisy}}$$

Tree-level potential relevant for EWPT,

$$V_0(h_u, h_d, s) = \frac{1}{32}(g_1^2+g_2^2)\left(h_u^2 - h_d^2\right)^2 + \frac{1}{4}\kappa^2 s^4 - \frac{1}{2}\lambda\kappa s^2 h_u h_d + \frac{1}{4}\lambda^2\left(h_d^2 h_u^2 + s^2\left(h_d^2 + h_u^2\right)\right)$$
$$+ \frac{\sqrt{2}}{6}\kappa A_\kappa s^3 - \frac{\sqrt{2}}{2}\lambda A_\lambda s h_u h_d + \frac{1}{2}m_d^2 h_d^2 + \frac{1}{2}m_u^2 h_u^2 + \frac{1}{2}m_s^2 s^2.$$

The zero temperature potential gets quantum contributions from all fields which couple with h_u, h_d and s.

In the R_ξ -gauge the one-loop CW corrections to the potential

$$\Delta V = \frac{1}{64\pi^2}\left(\sum_h n_h m_h^4(\xi)\left[\ln\left(\frac{m_h^2(\xi)}{Q^2}\right) - 3/2\right]\right.$$
$$+ \sum_V n_V m_V^4\left[\ln\left(\frac{m_V^2}{Q^2}\right) - 5/6\right]$$
$$- \sum_V \tfrac{1}{3} n_V (\xi m_V^2)^2\left[\ln\left(\frac{\xi m_V^2}{Q^2}\right) - 3/2\right]$$
$$\left. - \sum_f n_f m_f^4\left[\ln\left(\frac{m_f^2}{Q^2}\right) - 3/2\right]\right).$$

To avoid the large logarithms arising from CW one-loop correction consider only the light particles and integrate out the heavy ones and consider their threshold corrections (EFT approach).

Strategy

- NMSSM input parameters are given at M_{SUSY} scale. To avoid large logarithms, integrate out stop squarks below M_{SUSY} scale and consider the threshold corrections.

- Below M_{SUSY} scale, NMSSM tree-level potential can be described by the (2HDM+S) potential.

- Determine the matched conditions among the various model parameters of these two models.

- These NMSSM input parameters are evaluated at the M_{SUSY} scale in $\overline{\text{DR}}$-scheme. Run those (2HDM+S) model parameters using one-loop RG-running equations to the top scale. Convert those parameters to $\overline{\text{MS}}$-scheme.

- Calculate the total potential including thermal corrections

Matched conditions

The tree-level Z_3-symmetric (2HDM+S) potential,

$$V_0 = \frac{1}{2}\lambda_1 |H_d|^4 + \frac{1}{2}\lambda_2 |H_u|^4 + (\lambda_3 + \lambda_4) |H_d|^2 |H_u|^2 - \lambda_4 \left|H_u^\dagger H_d\right|^2 + \lambda_5 |S|^2 |H_d|^2$$
$$+ \lambda_6 |S|^2 |H_u|^2 + \lambda_7 \left(S^{*2} H_d \cdot H_u + h.c.\right) + \lambda_8 |S|^4 + m_1^2 |H_d|^2 + m_2^2 |H_u|^2$$
$$+ m_3^2 |S|^2 - m_4 (H_d \cdot H_u S + h.c.) - \frac{1}{3} m_5 \left(S^3 + h.c.\right).$$

Comparing the two tree-level potentials, at the scale $Q = M_{SUSY}$ the matched conditions are,

$$\lambda_1 = \frac{1}{4}\left(g'^2 + g^2\right), \quad \lambda_2 = \frac{1}{4}\left(g'^2 + g^2\right) + \Delta\lambda_2, \quad \lambda_3 = \frac{1}{4}\left(g^2 - g'^2\right),$$
$$\lambda_4 = \frac{1}{2}\left(2|\lambda|^2 - g^2\right), \quad \lambda_5 = \lambda_6 = |\lambda|^2, \quad \lambda_7 = -\lambda\kappa^*, \quad \lambda_8 = |\kappa|^2,$$
$$m_1^2 = m_{H_d}^2, \quad m_2^2 = m_{H_u}^2, \quad m_3^2 = m_S^2, \quad m_4 = A_\lambda \lambda, \quad m_5 = -A_\kappa \kappa.$$

$\Delta\lambda_2 \Rightarrow$ The only threshold corrections from stop squarks to h_u quartic at M_{SUSY} scale.

$$\Delta\lambda_2 = \frac{3 y_t^4 A_t^2}{8\pi^2 M_{SUSY}^2}\left(1 - \frac{A_t^2}{12 M_{SUSY}^2}\right).$$

Thermal correction

The one-loop finite-temperature potential,

$$V_{\rm th}^{i}(m_i^2(\Phi), T) = (-1)^F g_i \frac{T^4}{2\pi^2} J_{\mathsf{B/F}}\left(\frac{m_i^2(\Phi)}{T^2}\right)$$

with thermal functions

$$J_{\mathsf{B/F}}(y^2) = \int_0^\infty dx\ x^2\ \log\left[1 \mp \exp(-\sqrt{x^2+y^2})\right].$$

At the high-temperature limit,

$$\begin{aligned} J_B(y^2) &\approx & J_B^{\mathrm{high}-T}(y^2) = -\frac{\pi^4}{45} + \frac{\pi^2}{12}y^2 - \frac{\pi}{6}y^3 - \frac{1}{32}y^4 \log\left(\frac{y^2}{a_b}\right) \\ J_F(y^2) &\approx & J_F^{\mathrm{high}-T}(y^2) = \frac{7\pi^4}{360} - \frac{\pi^2}{24}y^2 - \frac{1}{32}y^4 \log\left(\frac{y^2}{a_f}\right) \end{aligned},$$

where $a_b = \pi^2 \exp(3/2 - 2\gamma_E)$ and $a_f = 16\pi^2 \exp(3/2 - 2\gamma_E)$.

If a light boson is added to the plasma with $m_i^2 \sim \phi^2$, then the $-y^3$ term in J_B will generate a negative cubic term $-\phi^3$ in the effective potential, which can generate an energy barrier between two degenerate vacua.

Thermal correction

$$V_{\rm eff}^{\rm dressed}(\Phi,T) = V_0 + \sum_i \left[V_{\rm CW}^i(m_i^2(\Phi)) + V_{\rm th}^i(m_i^2(\Phi),T) + V_{\rm ring}^i(m_i^2(\Phi),T) \right] ,$$

where,
$$V_{\rm ring}^i(m_i^2(\Phi),T) = -\frac{g_i T}{12\pi}\left(\left[m_i^2(\Phi)+\Pi_i\right]^{3/2} - \left[m_i^2(\Phi)\right]^{3/2} \right) .$$

Thermal corrections to the scalars and gauge bosons coming from the resumming the ring (or daisy) diagrams (resumming the IR-divergent contributions to the Matsubara zero mode propagator.)

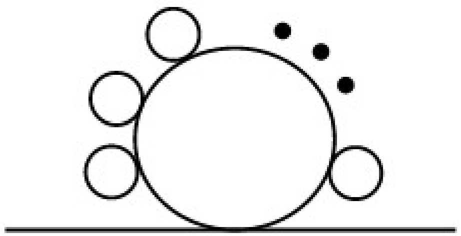

Daisy loop contribution to the self-energy for the scalar theory.

⇒ Arnold-Espinosa method

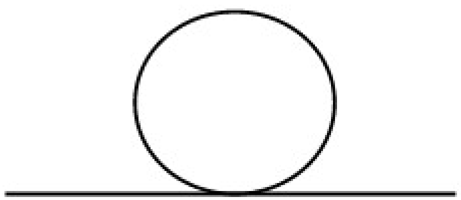

Quiros, hep-ph/9901312

Thermal masses

$\Pi(T^2) = C_{ij}T^2$, The Debye thermal corrections to the tree-level masses in the mass matrices

daisy coefficients

$$c_{H_u} = \tfrac{1}{48}\left(3g'^2 + 9g^2 + 12y_t^2 + 12\lambda_2 + 8\lambda_3 + 4\lambda_4 + 4\lambda_6\right),$$
$$c_{H_d} = \tfrac{1}{48}\left(3g'^2 + 9g^2 + 12y_b^2 + 4y_\tau^2 + 12\lambda_1 + 8\lambda_3 + 4\lambda_4 + 4\lambda_5\right),$$
$$c_S = \tfrac{1}{48}\left(8\lambda_5 + 8\lambda_6 + 16\lambda_8\right),$$
$$c_{W_{1,2,3}} = 2g^2,$$
$$c_B = 2g'^2$$

The gauge symmetries plus the discrete Z_3 -symmetry of NMSSM set the off-diagonal terms of the $\Pi(T^2)$ matrix to zero.

SFOPT and Nucleation criterion

- To avoid baryon asymmetry generated at the EWPT being wash out, the PT must be strongly first order $\Rightarrow \gamma_{EW} = \frac{v_{EW}}{T_c} \gtrsim 1.0$
(Sphaleron process is suppressed enough inside the broken electroweak phase)

- The Hubble parameter $\mathcal{H}(T)$ as $\mathcal{H}^{-4}(T) = (M^*_{Pl}/T^2)^4$.

- The bubble nucleation rate in a unit space-volume has the form

$$\Gamma(T) \simeq A(T) \exp(-S_3(T)/T) \, ,$$

where $A(T) \simeq T^4$, $S_3(T)$ is the free energy of the critical bubble at a given temperature.

- The probability that the bubble is nucleated inside a causal volume reads $P \sim \Gamma \cdot \mathcal{H}^{-4} \sim \frac{M^{*4}_{Pl}}{T^4} \exp(-S_3/T)$

- The first bubble nucleates when $P \sim 1$,
$\Rightarrow$nucleation criterion, $S_3(T)/T \sim 4 \ln\left(\frac{M^*_{Pl}}{T}\right) \sim 150$, where $T \simeq M_{EW}$.
More accurate calculation reveals $S_3(T_c)/T_c \simeq 135$

Toolbox

Use CosmoTransitions to calculate the critical temperature (T_c), nucleation temperature (T_n), etc..

uses path deformation method to find the critical bubble profile

C. Wainwright, [arXiv:1109.4189]

Use NMSSMTools to calculate the spectrum and check various theoretical, dark matter and collider experiental bounds

Use HiggsSignals, HiggsBounds to check the Higgs sector constraints.

Use CheckMATE and SModelS to check the viability of benchmark points under LHC experimental searches.

Constraints on SFOEWPT favoured parameter space in NMSSM

FT loop calculation indicates preference for relatively light singlet-like and doublet-like Higgs masses which tend to become EWPT first order and strong

Carena et al., Phys.Rev.D 85 (2012) 036003
Kozaczuk et al., Phys.Rev.D 87 (2013) 7, 075011
Huang et al, Phys.Rev.D 91 (2015) 2, 025006

m_{a_S, h_S}

$m_{A,H}$ $\Longrightarrow$ Relatively low κ, A_κ

low A_λ

Athron et al., JHEP 11 (2019) 151
Baum et al., JHEP 03 (2021) 055

Constraints on SFOEWPT parameter space

- SM-like Higgs Boson precision study
- BSM heavy Higgs searches

(in the tb (for $H^\pm$) and $\tau\tau$ (for H, A) final states) $\Longrightarrow (m_A - \tan\beta)$

$\longrightarrow$ Light $m_{H,A,H^\pm}$ $\Longleftrightarrow$ low $\tan\beta$

larger λ , smaller κ

$v_S \backsim$ EW scale

$\Bigg\}$ light $\widetilde{S}$

$m_{\widetilde{S}} = 2\kappa v_S$

$= 2\kappa \frac{\mu_{eff}}{\lambda}$

$\Longrightarrow$ Possible Dark Matter $\Bigg\}$ $\longrightarrow$ DM relic density, Constraints from DMDD-SI and DMDD-SD cross-section

Constraints from the Higgs seaches

ATLAS TWIKI

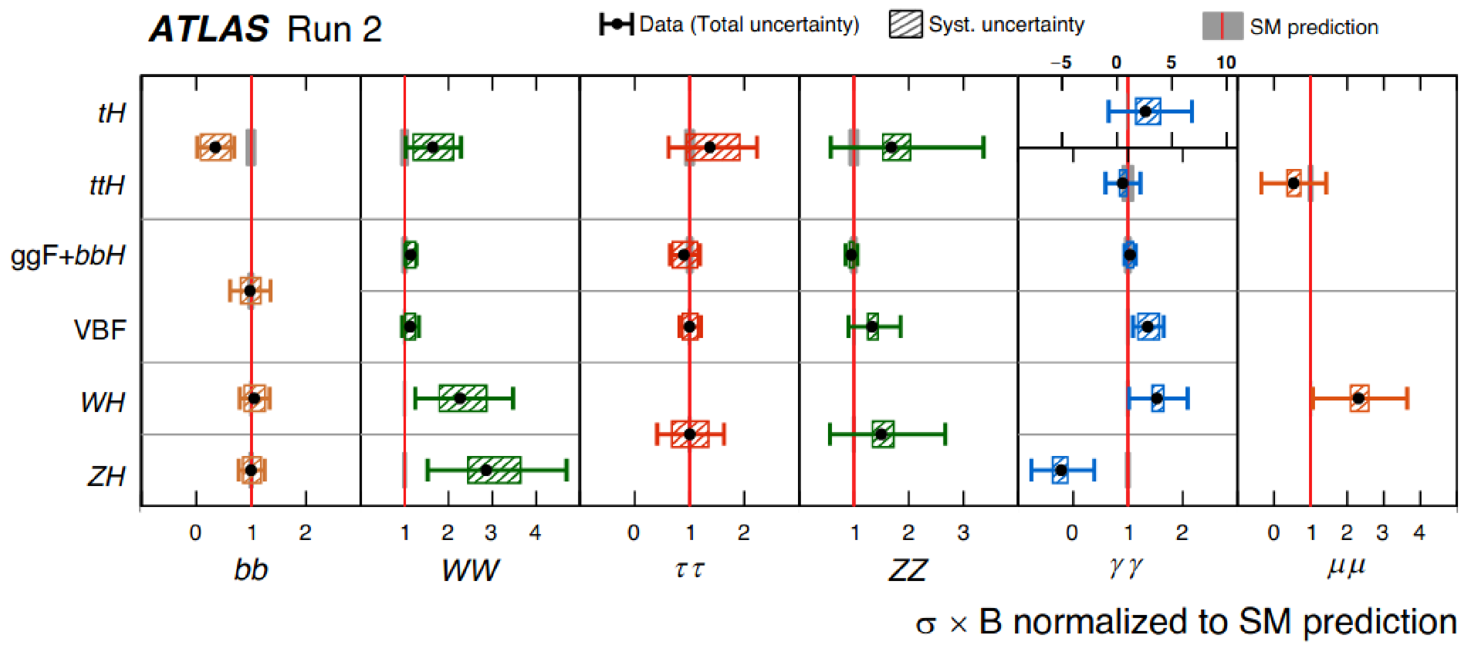

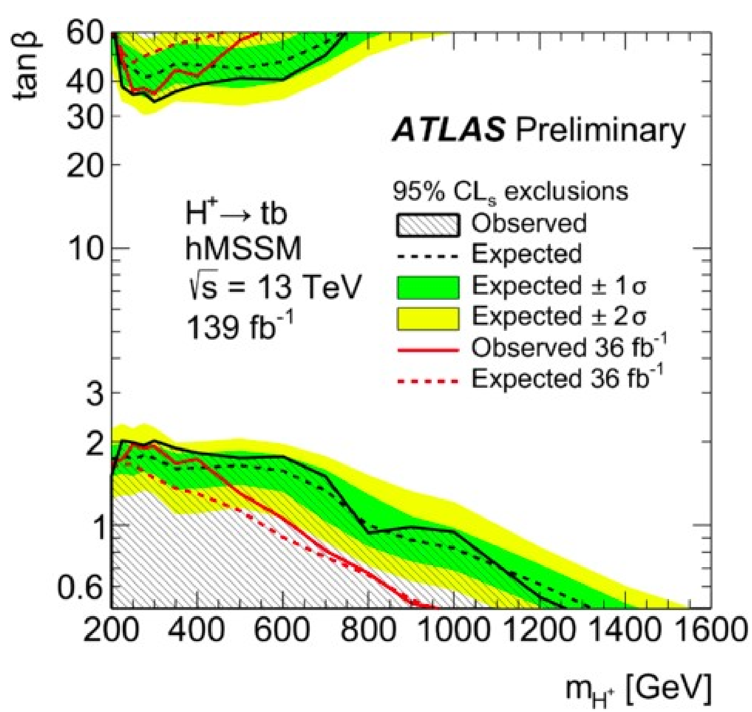

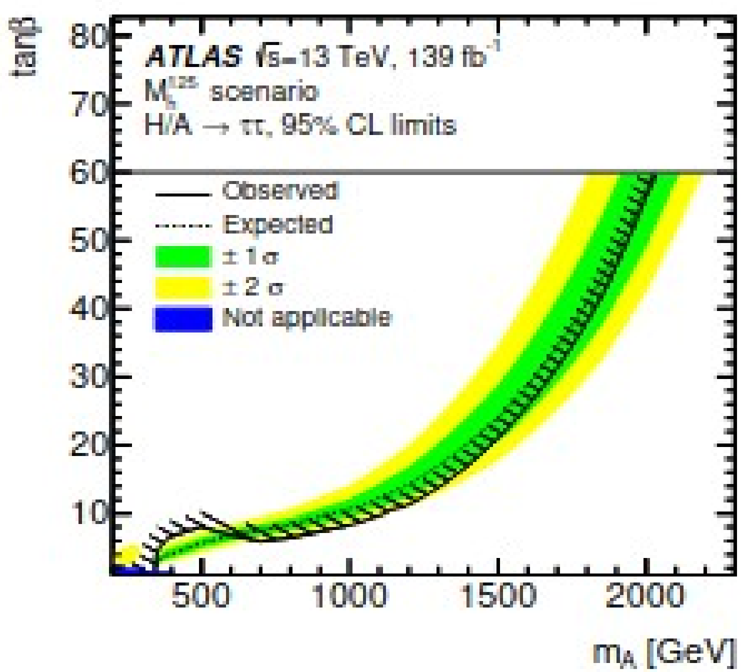

Constraints from the Dark Matter direct detection

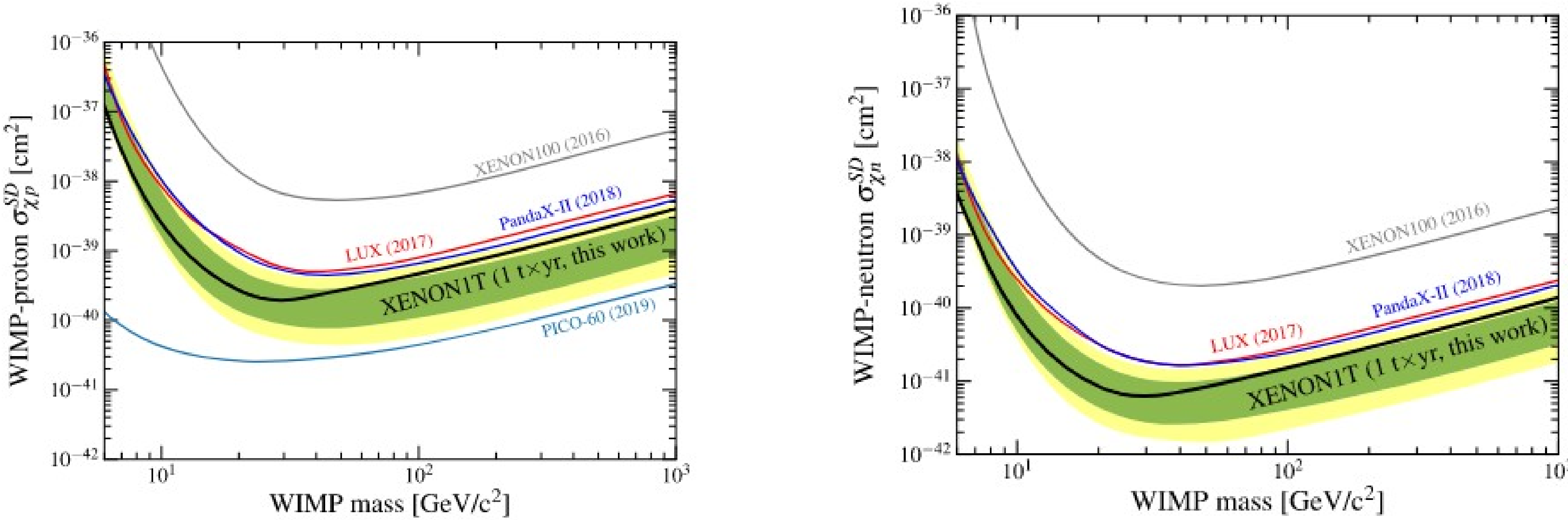

Constraints from Ewino sector

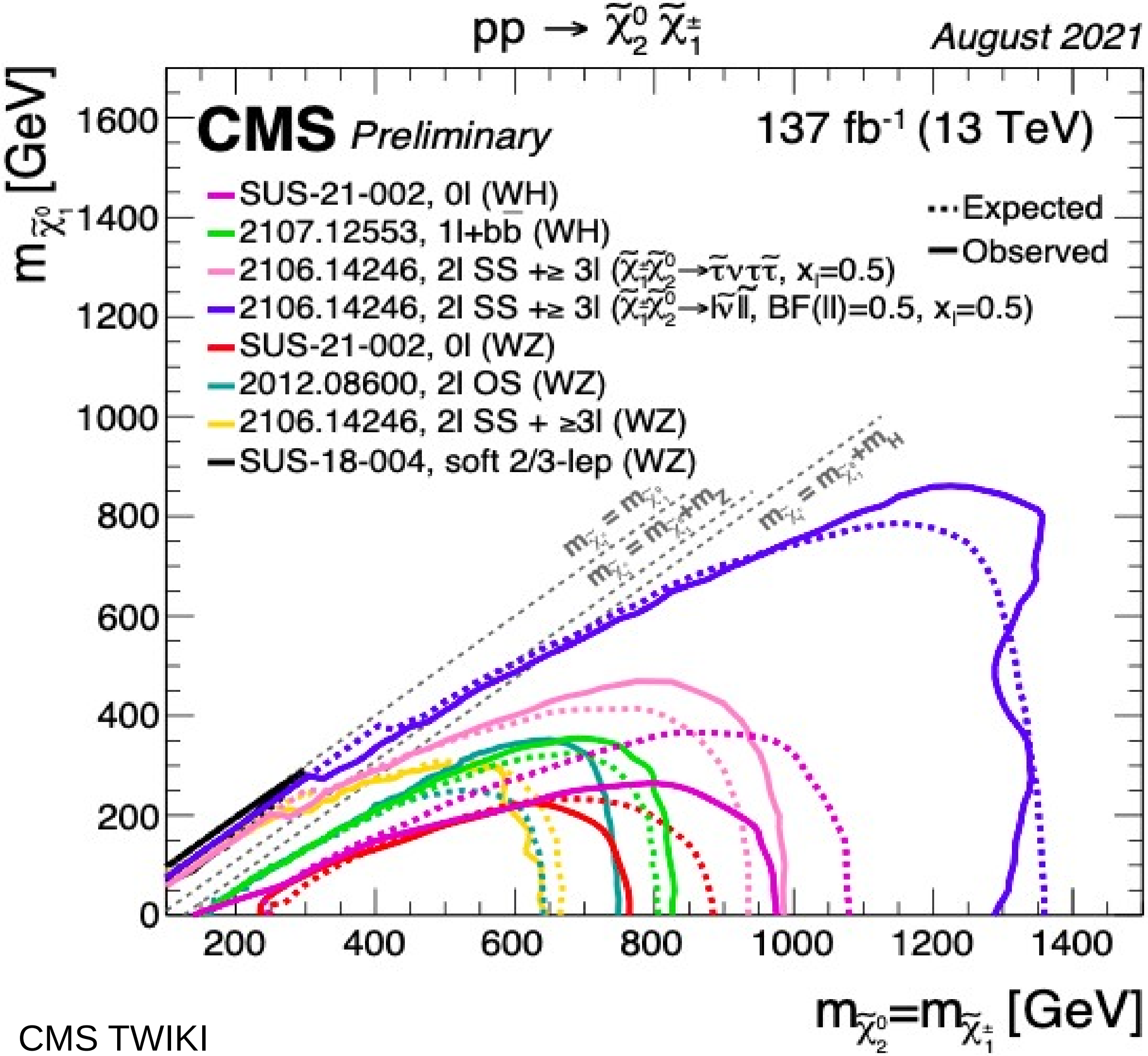

CMS TWIKI

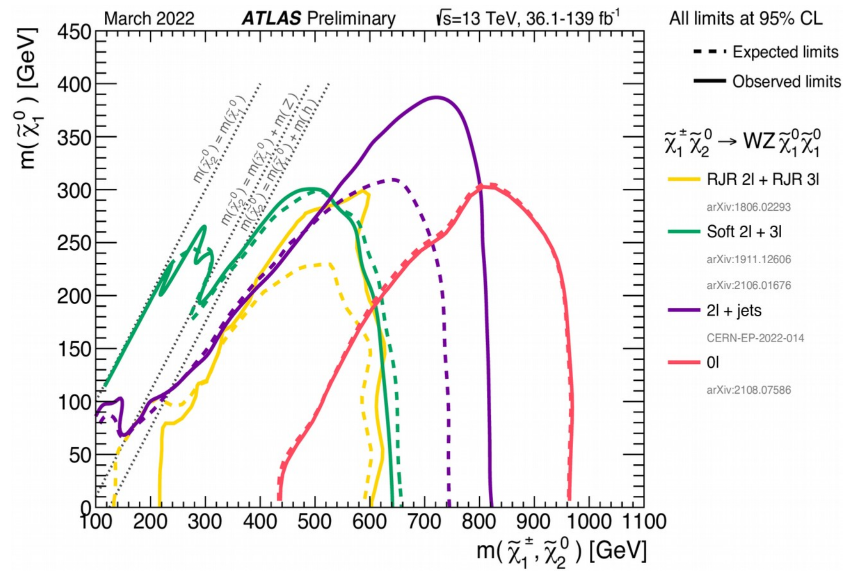

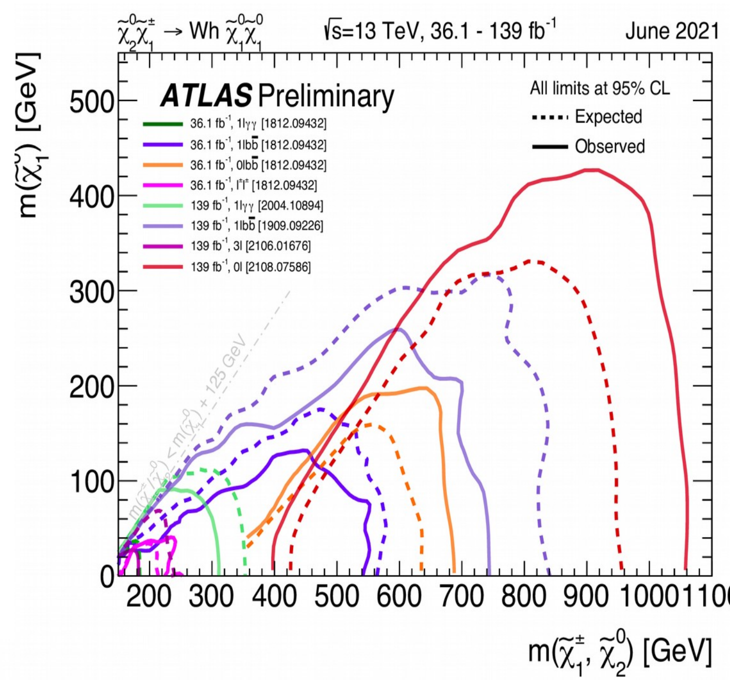

ATLAS TWIKI

Electroweakino searches put constraints on the the parameter space with relatively low $\mu_{\rm eff}$ (Higgsino-like states), relatively light bino and singlino-like states.

Parameter space scan

Use NMSSMTools to scan SFOEWPT motivated region of parameter space

λ	$\lvert\kappa\rvert$	$\tan\beta$	$\lvert\mu_{\rm eff}\rvert$ (GeV)	$\lvert A_\lambda\rvert$ (TeV)	$\lvert A_\kappa\rvert$ (GeV)	$\lvert M_1\rvert$ (GeV)	$\lvert A_t\rvert$ (TeV)	$m_{\tilde{Q}_3}$ (TeV)	$m_{\tilde{U}_3}$ (TeV)
0.2–0.7	≤ 0.5	1–20	≤ 500	≤ 2	≤ 200	≤ 500	≤ 5	2–5	2–5

$m_{\tilde{g}}, m_{\tilde{f}_{1,2}} = 5$ TeV;
$m_{\tilde{f}_3} = 5.5$ TeV;
$m_{\widetilde{W}} = 2.5$ TeV

Constraints implemented NMSSMTools

Planck-reported 2σ range upper bound on relic density, i.e., $\Omega h^2 \leq 0.131$

Considered latest spin-independent (SI) and spin-dependent (SD) bounds

XENON Collaboration, PRL 121(2018) 11, 111302

XENON Collaboration, PRL 122 (2019) 14, 141301

PICO Collaboration, PRD 100 (2019) 2, 022001

Used NMSSMTools LHC bound for $pp \to \chi_1^\pm \chi_2^0 \to WZ\not{E}_T \to 3\ell + \not{E}_T$ final state.

CMS Collaboration, JHEP 03 (2018)

Various Flavor physics constraints

Have not considered muon (g − 2) constraints (have taken heavy smuon).

In addition, up-to-date constraints pertaining to the observed Higgs sector are checked via dedicated packages like HiggsBounds-v5.8.0 and HiggsSignals-v2.5.0.

Allowed primary sample

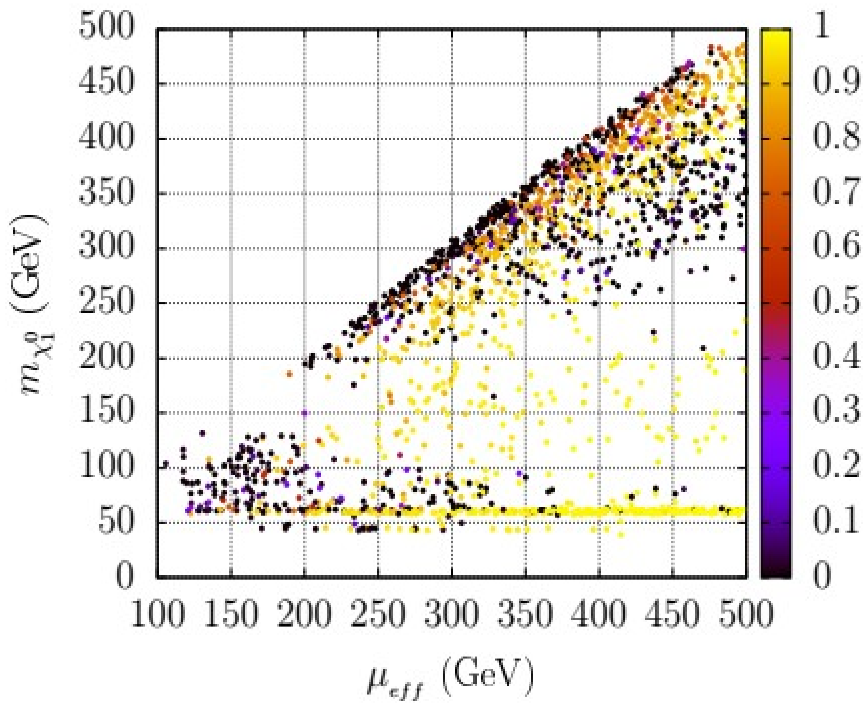

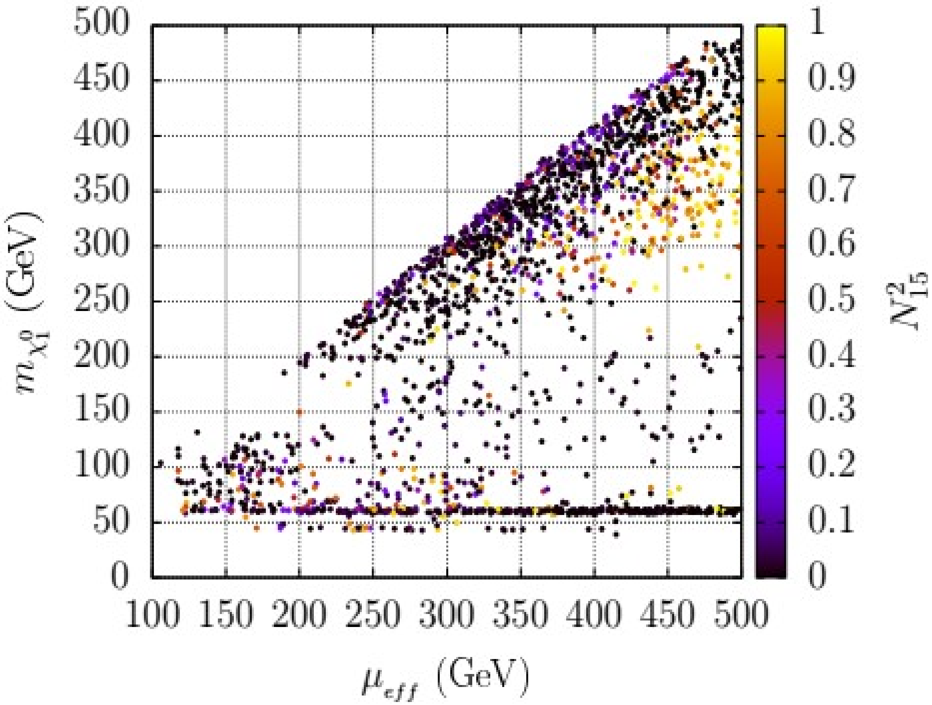

All points pass relevant Higgs and Dark Matter constraints

Significant amount of SFOEWPT favoured parameter space is ruled out

Electroweakino searches at the LHC would rule out more parameter points

Relevant experimental analyses implemented in CheckMate and SModelS

Analysis (Luminosity)	Process	Final State	SModelS	CheckMATE
CMS-SUS-17-004 [167] (35.9 fb^{-1})	$\chi_2^0\chi_1^\pm \to Z/h_{\rm SM}\,\chi_1^0 W^\pm \chi_1^0$	$(m \geq 0)\ell + (n \geq 0)\tau + \not{E}_T$		✓
CMS-SUS-16-048 [168] (35.9 fb^{-1})	$\tilde{t}\tilde{t} \to b\chi_1^\pm b\chi_1^\pm$ $\chi_2^0\chi_1^\pm \to Z^*\chi_1^0\, W^{\pm *}\chi_1^0$	$(k \geq 0)\ell + (m \geq 0)b + (n \geq 0)$-jet$+\not{E}_T$		✓
CMS-SUSY-16-039 [169] (35.9 fb^{-1})	$\chi_2^0\chi_1^\pm \to \ell\tilde{\ell}\ell\tilde{\nu}$ $\chi_2^0\chi_1^\pm \to \tilde{\ell}\ell\tilde{\tau}\nu$ $\chi_2^0\chi_1^\pm \to \tilde{\tau}\tau\tilde{\tau}\nu$ $\chi_2^0\chi_1^\pm \to Z\chi_1^0\, W^\pm\chi_1^0$ $\chi_2^0\chi_1^\pm \to h_{\rm SM}\chi_1^0\, W^\pm\chi_1^0$	$(n \geq 0)\ell + \not{E}_T$	✓	✓
CMS-SUS-17-010 [170] (35.9 fb^{-1})	$\chi_1^\pm\chi_1^\mp \to W^\pm\chi_1^0\, W^\mp\chi_1^0$ $\chi_1^\pm\chi_1^\mp \to \nu\tilde{\ell}\,\ell\tilde{\nu}$	$2\ell + \not{E}_T$	✓	
CMS-SUS-16-043 [171] (35.9 fb^{-1})	$\chi_2^0\chi_1^\pm \to h_{\rm SM}\chi_1^0\, W^\pm\chi_1^0$	$1\ell + 2b + \not{E}_T$	✓	
CMS-SUS-16-045 [172] (35.9 fb^{-1})	$\chi_2^0\chi_1^\pm \to h_{\rm SM}\chi_1^0\, W^\pm\chi_1^0$	$1\ell + 2\gamma + \not{E}_T$	✓	
CMS-SUS-16-034 [173] (35.9 fb^{-1})	$\chi_2^0\chi_1^\pm \to Z/h_{\rm SM}\,\tilde{\chi}_1^0\, W^\pm\chi_1^0$	$(m \geq 2)\ell + (n \geq 1)$-jet$+\not{E}_T$	✓	
ATLAS-1712-08119 [174] (36.1 fb^{-1})	$\tilde{\ell}\tilde{\ell}$ $\chi_2^0\chi_1^\pm \to Z^*\chi_1^0\, W^*\chi_1^0$	$2\ell + (n \geq 0)$-jet$+\not{E}_T$		✓
ATLAS-1803-02762 [175] (35.9 fb^{-1})	$\chi_2^0\chi_1^\pm \to Z\chi_1^0\, W^\pm\chi_1^0$ $\chi_2^0\chi_1^\pm \to \nu\tilde{\ell}\ell\tilde{\ell}$ $\chi_1^\pm\chi_1^\mp \to \nu\tilde{\ell}\nu\tilde{\ell}$	$(n \geq 2)\ell + \not{E}_T$	✓	✓
ATLAS-1812-09432 [176] (36.1 fb^{-1})	$\chi_2^0\chi_1^\pm \to h_{\rm SM}\chi_1^0\, W^\pm\chi_1^0$	$(j \geq 0)\ell + (k \geq 0)$-jet $+(m \geq 0)b + (n \geq 0)\gamma + \not{E}_T$	✓	
ATLAS-1806-02293 [177] (36.1 fb^{-1})	$\chi_2^0\chi_1^\pm \to Z\chi_1^0\, W^\pm\chi_1^0$	$(m \geq 2)\ell + (n \geq 0)$-jet$+\not{E}_T$	✓	
ATLAS-1909-09226 [178] (139 fb^{-1})	$\chi_2^0\chi_1^\pm \to h_{\rm SM}\chi_1^0\, W^\pm\chi_1^0$	$1\ell + 2b + \not{E}_T$	✓	
ATLAS-1912-08479 [179] (139 fb^{-1})	$\chi_2^0\chi_1^\pm \to Z(\to \ell\ell)\,\tilde{\chi}_1^0\;\; W(\to \ell\nu)\,\tilde{\chi}_1^0$	$3\ell + \not{E}_T$	✓	✓
ATLAS-1908-08215 [180] (139 fb^{-1})	$\tilde{\ell}\tilde{\ell}$ $\chi_1^\pm\chi_1^\mp\,(\chi_1^\pm \to W^\pm\chi_1^0)$ $(\chi_1^\pm \to \tilde{\ell}\nu/\tilde{\nu}\ell)$	$2\ell + \not{E}_T$	✓	✓
ATLAS-1911-12606 [181] (139 fb^{-1})	$\tilde{\ell}\tilde{\ell}$ $\chi_1^\pm\chi_2^0 \to W^*(\to qq)\;\chi_1^0\;\; Z^*(\to ll)\;\chi_1^0$	jets $+ 2\ell + \not{E}_T$		✓
ATLAS-2004-10894 [182] (139 fb^{-1})	$\chi_2^0\chi_1^\pm \to h_{\rm SM}(\to \gamma\gamma)\;\chi_1^0\; W(\to \ell\nu)\chi_1^0$	$1\ell + 2\gamma + \not{E}_T$	✓	✓

Disallowed scenarios with low μ_{eff}

Inputs/Observables	BP-D1	BP-D2	BP-D3
λ, κ, $\tan\beta$	0.683, 0.060, 4.77	0.547, 0.044, 2.87	0.565, 0.071, 2.87
A_λ, A_κ (GeV)	-1352.3, 134.5	978.4, -110.0	963.5, -112.5
$\mu_{\rm eff}$, M_1 (GeV)	-274.4, 478.8	308.0, 460.3	308.0, -57.2
$m_{\chi^0_{1,2,3,4},\chi^\pm_1}$ (GeV)	60.9, -304.3, 307.9, 479.4, -284.1	60.6, 312.7,-338.3, 468.1, 316.3	-59.6, 91.1, 327.2, -338.4, 316.0
$m_{h_1,h_2,a_1,H^\pm}$ (GeV)	79.2, 124.4, 126.6, 1359.0	78.1, 122.2, 109.5, 963.8	86.9, 123.0, 142.6, 963.6
Ωh^2	4.9×10^{-4}	4.4×10^{-4}	4.8×10^{-3}
$\sigma^{\rm SI}_{\chi^0_1-p(n)}\times\xi$ (cm^2)	$4.5(4.6)\times10^{-47}$	$2.4(2.5)\times10^{-47}$	$2.5(2.6)\times10^{-47}$
$\sigma^{\rm SD}_{\chi^0_1-p(n)}\times\xi$ (cm^2)	$3.5(3.2)\times10^{-42}$	$7.6(5.8)\times10^{-43}$	$1.9(1.5)\times10^{-43}$
First T_c (GeV)	129.4 / 1st-order	151.5 / 1st-order	165.7 / 1st-order
$\{h_d,h_u,s\}_{\rm False\_vac.}$ (GeV)	$\{0,\ 0,\ 0\}$	$\{0,\ 0,\ 0\}$	$\{0,\ 0,\ 0\}$
$\{h_d,h_u,s\}_{\rm True\_vac.}$ (GeV)	$\{25.5, 145.6, -474.4\}$	$\{0, 0, 539.9\}$	$\{0, 0, 557.5.9\}$
Second T_c (GeV)	–	112.7 / 2nd-order	105.6 / 1st-order
$\{h_d,h_u,s\}_{\rm False\_vac.}$ (GeV)	–	$\{0,\ 0, 661.7\}$	$\{0,\ 0, 662.3\}$
$\{h_d,h_u,s\}_{\rm True\_vac.}$ (GeV)	–	$\{9.5, 31.5, 668.2\}$	$\{12.8, 41.6, 669.0\}$
T_n (GeV) (Nucleation)	No nucleation	96.2 / 1st-order	55.9 / 1st-order
$\{h_d,h_u,s\}_{\rm False\_vac.}$ (GeV)	–	$\{0,\ 0,\ 0\}$	$\{0,\ 0,\ 0\}$
$\{h_d,h_u,s\}_{\rm True\_vac.}$ (GeV)	–	$\{67.0, 197.8, 774.8\}$	$\{68.1, 199.2, 759.2\}$
$\gamma_{\rm EW}=\Delta_{SU(2)}/T_n$	–	2.2	3.8
CheckMATE result	Excluded	Excluded	Excluded
r-value	1.12	1.01	2.13
Analysis ID	CMS_SUS_16_039	CMS_SUS_16_039	CMS_SUS_16_039
Signal region ID	SR_A30	SR_A30	SR_G05

‘Nucleation is More than Critical’ Baum et al., JHEP 03 (2021) 055

Exclusion of Parameter space of $\mu_{eff}\lesssim$300 GeV with light singlino/bino -like states from the electroweakino searches.

Allowed benchmark scenarios

Input/Observables	BP-A1	BP-A2	BP-A3
λ, κ, $\tan\beta$ A_λ, A_κ (GeV) $\mu_{\rm eff}$, M_1 (GeV)	0.609, 0.326, 1.98 477.0, 37.8 421.8, 365.1	0.633, 0.216, 1.79 −558.7, −46.3 −398.7, 286.3	0.523, 0.041, 3.65 −1253.9, 138.1 −334.5, −143.8
$m_{\chi^0_{1,2,3,4}, \chi^\pm_1}$ (GeV) $m_{h_1,h_2,a_1,H^\pm}$ (GeV)	−360.9, 415.1, −447.5, 493.2, 431.5 122.7, 449.0, 79.0, 818.4	284.5, −289.5, −421.8, −426.9, −412.1 126.9, 288.5, 84.8, 800.9	−61.3, −139.2, −359.3, 359.7, −345.3 74.0, 124.7, 121.0, 1293.3
Ωh^2 $\sigma^{\rm SI}_{\chi^0_1-p(n)} \times \xi$ (cm^2) $\sigma^{\rm SD}_{\chi^0_1-p(n)} \times \xi$ (cm^2)	0.107 $7.2(7.6) \times 10^{-48}$ $9.4(7.3) \times 10^{-42}$	0.119 $1.2(1.2) \times 10^{-46}$ $3.5(2.8) \times 10^{-42}$	1.96×10^{-3} $4.1(4.3) \times 10^{-47}$ $1.1(0.8) \times 10^{-41}$
CheckMATE result r-value Analysis ID Signal region ID	Allowed 0.08 CMS_SUS_16_039 SR_A08	Allowed 0.14 CMS_SUS_16_039 SR_A28	Allowed 0.55 CMS_SUS_16_039 SR_A31

Relatively large μ_{eff} passes the constraints from the electroweakino seraches in LHC

LSP DM can be highly bino or singlino-like and its relic abundance can fall within the Planck-observed band.

Under favorable circumstances, down to μ_{eff} ~335 GeV could survive

Phase diagrams

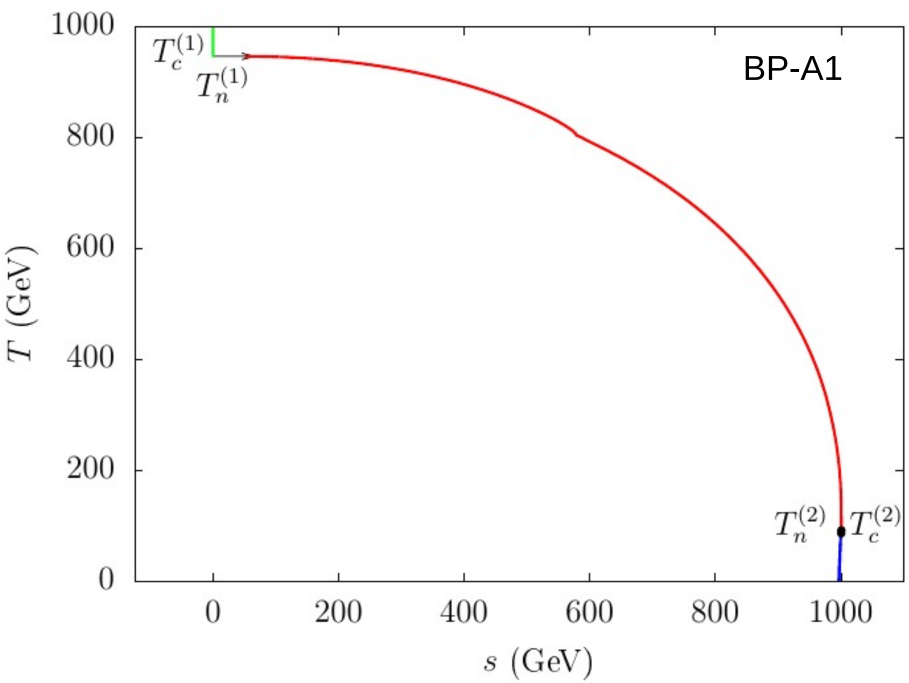

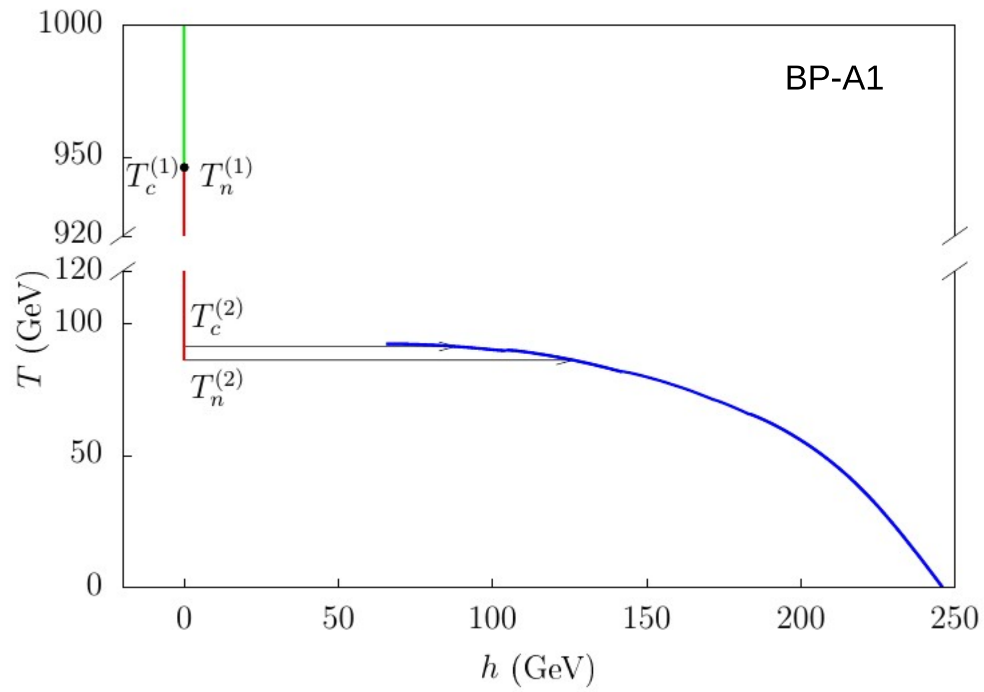

BM No.	T_i (GeV) (Transition pattern)		$\{h_d, h_u, h_s\}_{\text{false}}$ (GeV)	$\xrightarrow{\text{Transition}}$ type	$\{h_d, h_u, h_s\}_{\text{true}}$ (GeV)	$\gamma_{\text{EW}} = \frac{\Delta_{SU(2)}}{T_n}$
BP-A1	T_c	946.0	{0, 0, 0}	,,	{0, 0, 64.4}	
	II-S(1)-D(1)	91.3	{0, 0, 1000.9}	,,	{39.9, 78.6, 1000.6}	
	T_n	945.6	{0, 0, 0}	,,	{0, 0, 66.2}	
	II-S(1)-D(1)	86.2	{0, 0, 1000.8}	,,	{57.1, 112.5, 1000.3}	1.46

Phase diagrams

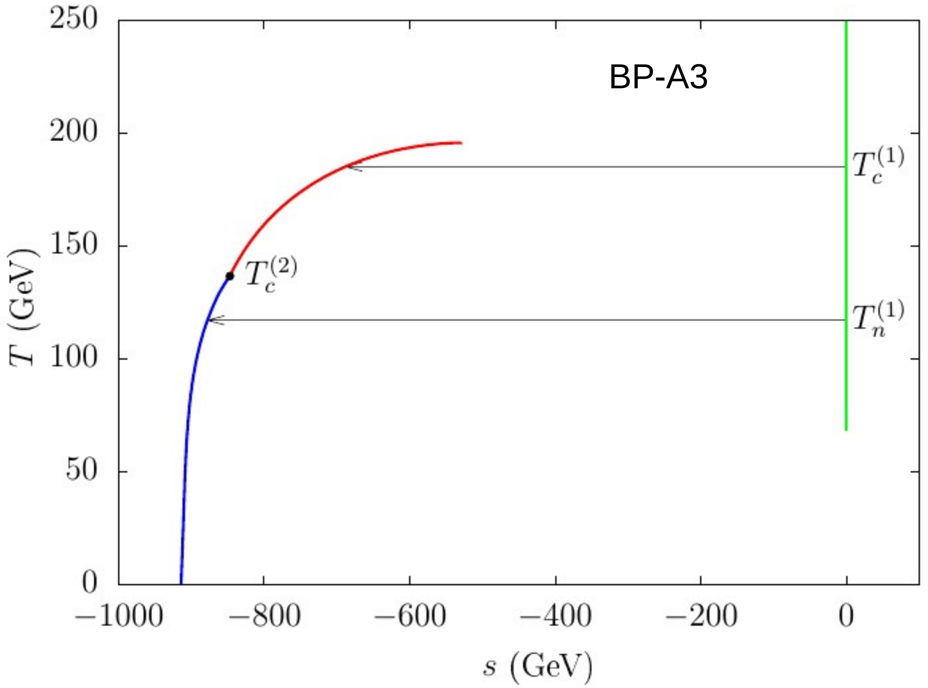

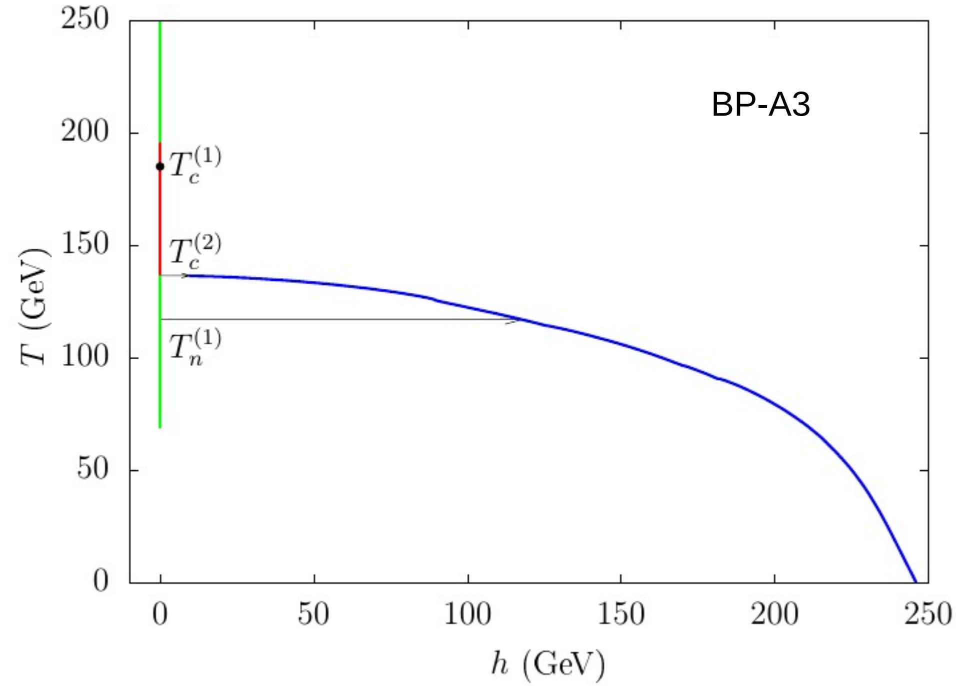

BM No.	T_i (GeV) (Transition pattern)		$\{h_d, h_u, h_s\}_{\text{false}}$ (GeV)	Transition type	$\{h_d, h_u, h_s\}_{\text{true}}$ (GeV)	$\gamma_{\text{EW}} = \frac{\Delta_{SU(2)}}{T_n}$
BP-A3	T_c II-S(1)-D(2)	185.0	$\{0, 0, 0\}$	,,	$\{0, 0, -668.9\}$	
		136.5	$\{0, 0, -846.6\}$	SO	$\{2.3, 9.1, -846.7\}$	
	T_n I-(1)	116.9	$\{0, 0, 0\}$	FO	$\{30.3, 113.8, -877.4\}$	1.01

Pattern of Phase Transition

BM No.	T_i (GeV) (Transition pattern)		$\{h_d, h_u, h_s\}_{\text{false}}$ (GeV)	$\xrightarrow{\text{Transition}}$ type	$\{h_d, h_u, h_s\}_{\text{true}}$ (GeV)	$\gamma_{\text{EW}} = \frac{\Delta_{SU(2)}}{T_n}$
BP-A1	T_c	946.0	$\{0, 0, 0\}$	,,	$\{0, 0, 64.4\}$	
	`II-S(1)-D(1)`	91.3	$\{0, 0, 1000.9\}$	,,	$\{39.9, 78.6, 1000.6\}$	
	T_n	945.6	$\{0, 0, 0\}$	,,	$\{0, 0, 66.2\}$	
	`II-S(1)-D(1)`	86.2	$\{0, 0, 1000.8\}$	,,	$\{57.1, 112.5, 1000.3\}$	1.46
BP-A2	T_c	644.4	$\{0, 0, 0\}$	,,	$\{0, 0, -100.0\}$	
	`II-S(1)-D(1)`	95.8	$\{0, 0, -916.3\}$	,,	$\{41.4, 72.9, -915.3\}$	
	T_n	644.3	$\{0, 0, 0\}$	,,	$\{0, 0, -104.8\}$	
	`II-S(1)-D(1)`	94.5	$\{0, 0, -914.9\}$	,,	$\{48.5, 85.6, -914.8\}$	1.04
BP-A3	T_c	185.0	$\{0, 0, 0\}$	,,	$\{0, 0, -668.9\}$	
	`II-S(1)-D(2)`	136.5	$\{0, 0, -846.6\}$	SO	$\{2.3, 9.1, -846.7\}$	
	T_n `I-(1)`	116.9	$\{0, 0, 0\}$	FO	$\{30.3, 113.8, -877.4\}$	1.01

For μ_{eff} on the larger side, a two-step phase transition is a more likely phenomenon with the first transition taking place in the singlet field direction followed by the other in the SU(2) field directions.

Typical when the trivial and the global minima are much separated in field space. Larger μ_{eff} corresponds to a larger v_S at zero temperature for a given λ, a feature that governs the field-separation at T_C.

Gravitational waves from FOPT

The dynamics of the nucleated bubbles generated from FOPT could generate stochastic background of gravitational waves (GW).

It is caused mainly by three mechanisms namely,

(i) bubble collisions,

(ii) sound waves induced by the bubbles running through the cosmic plasma

(iii) Magnetohydrodynamic turbulence induced by the bubble expansions in the cosmic plasma.

$$\Omega_{\rm GW}h^2 \simeq \Omega_\phi h^2 + \Omega_{\rm sw}h^2 + \Omega_{\rm turb}h^2$$

sourced by
collisions of bubble walls

Kosowsky, et. al., PRL 69 (1992) 2026;
PRD 45 (1992) 4514
Huber, Konstandin, JCAP 0809 (2008) 022

sourced by
plasma sounds waves
(usually the dominent one)

Hindmarsh, et. al., PRL 112 (2014) 041301;
Hindmarsh, Hijazi, JCAP 12 (2019) 062

sourced by
plasma turbulence

Gogoberidze, et. al., PRD 76 (2007) 083002
Caprini, at. al., JCAP 0912 (2009) 024

The contribution of bubble collision may be ignored since long-lasting sound waves during and after the FOPT contribute mostly to the production of gravitational waves, followed by MHD turbulence.

Observables for GW calculation from FOPT

Important quatities:

$$\alpha = \frac{\rho_{\rm vac}}{\rho^*_{\rm rad}} = \frac{1}{\rho^*_{\rm rad}}\left[T\frac{\Delta \dot{V}(T)}{\dot{T}} - \Delta V(T)\right]\Bigg|_{T_n}$$

Related to the energy budget of the FOPT

$$\beta = -\frac{dS_3(T)}{dt}\Big|_{t_n} \simeq H_n T_n \frac{d(S_3(T)/T)}{dT}\Big|_{T_n}$$

Related to the inverse duration of the transition

v_w the wall-velocity of the expanding bubble

T_n Nucleation Temperature

BP No.	T_n (GeV)	α	β/H_n
BP-A1	945.9	2.15×10^{-5}	1.19×10^{7}
	86.2	4.33×10^{-2}	1.21×10^{3}
BP-A2	644.3	1.12×10^{-4}	2.06×10^{6}
	94.5	1.82×10^{-2}	3.71×10^{4}
BP-A3	116.9	8.63×10^{-2}	2.22×10^{2}

For this work, we consider v_w value 1.

GW from sound waves

$$\Omega_{\rm sw}h^2 = 2.65\times10^{-6}\,\Upsilon(\tau_{\rm sw})\left(\frac{\beta}{H_\star}\right)^{-1} v_w\left(\frac{\kappa_v\alpha}{1+\alpha}\right)^2\left(\frac{g_*}{100}\right)^{-\frac{1}{3}}\left(\frac{f}{f_{\rm sw}}\right)^3\left[\frac{7}{4+3\left(\frac{f}{f_{\rm sw}}\right)^2}\right]^{\frac{7}{2}}$$

Peak value

$$f_{\rm sw} = 1.9\times10^{-5}\,{\rm Hz}\left(\frac{1}{v_w}\right)\left(\frac{\beta}{H_\star}\right)\left(\frac{T_n}{100\,{\rm GeV}}\right)\left(\frac{g_*}{100}\right)^{\frac{1}{6}}$$

$$\Upsilon(\tau_{\rm sw}) = 1-\frac{1}{\sqrt{1+2\tau_{\rm sw}H_*}}$$

due to the finite lifetime of the sound waves

Hindmarsh et al., arXiv:2008.09136
Guo et al., JCAP 01 (2021)

$$\kappa_v \simeq \left[\frac{\alpha}{0.73+0.083\sqrt{\alpha}+\alpha}\right]$$

Fraction of energy from the PT converted into the bulk motion of the plasma

Note that, peak frequency proportinal with $\frac{\beta}{H_\star}$ and T_n

GW power spectrum due to sound wave from beyond the bag model

Replace: $\frac{\alpha\kappa_\nu}{\alpha+1} \rightarrow \left(\frac{D\bar{\theta}}{4e_s}\right)\kappa_{\bar{\theta}}$

Giese, Konstandin and van de Vis, JCAP 07 (2020)

GW from MHD turbulence

$$\Omega_{\rm turb}h^2 = 3.35\times10^{-4}\left(\frac{\beta}{H_*}\right)^{-1}\left(\frac{\kappa_{\rm turb}\alpha}{1+\alpha}\right)^{\frac{3}{2}}\left(\frac{100}{g_*}\right)^{\frac{1}{3}} v_w\frac{(f/f_{\rm turb})^3}{[1+(f/f_{\rm turb})]^{\frac{11}{3}}(1+8\pi f/h_*)}$$

$$f_{\rm turb} = 2.7\times10^{-5}\,{\rm Hz}\,\frac{1}{v_w}\left(\frac{\beta}{H_*}\right)\left(\frac{T_*}{100\,{\rm GeV}}\right)\left(\frac{g_*}{100}\right)^{\frac{1}{6}}$$

SNR $= \sqrt{\delta\times\mathcal{T}\int_{f_{min}}^{f_{max}} df\left[\frac{h^2\Omega_{\rm GW}(f)}{h^2\Omega_{\rm exp}(f)}\right]^2}$

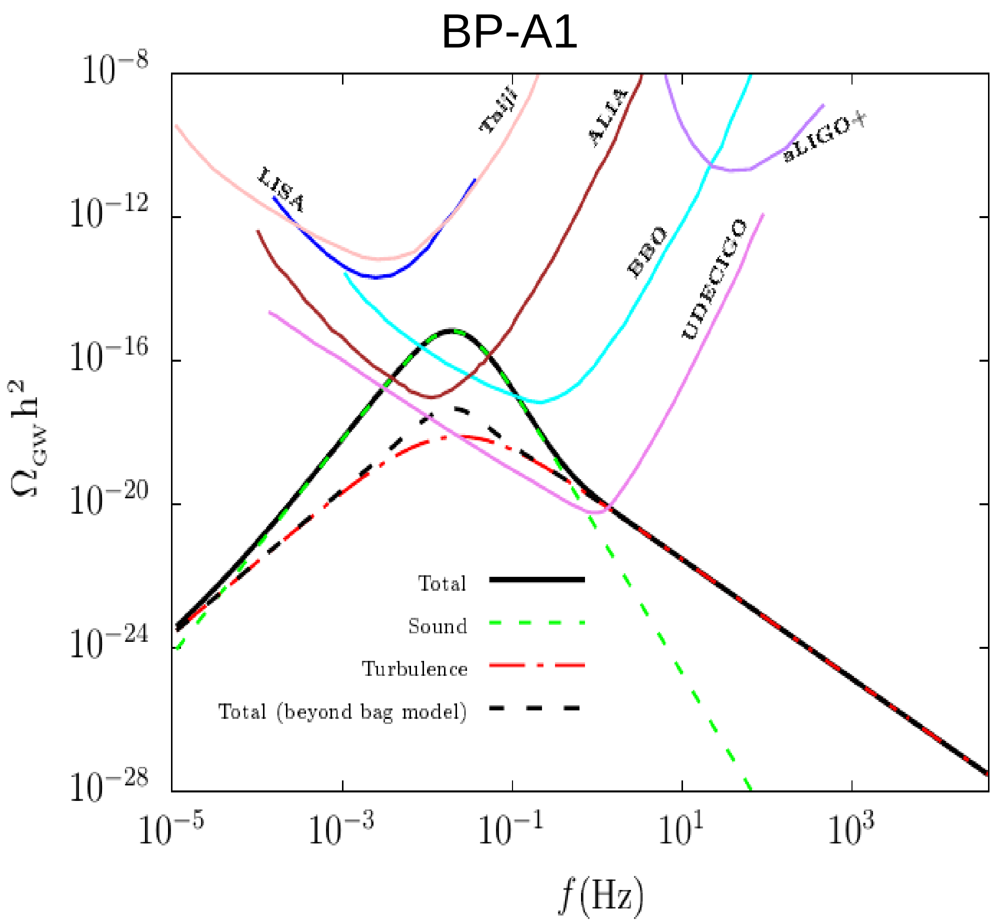

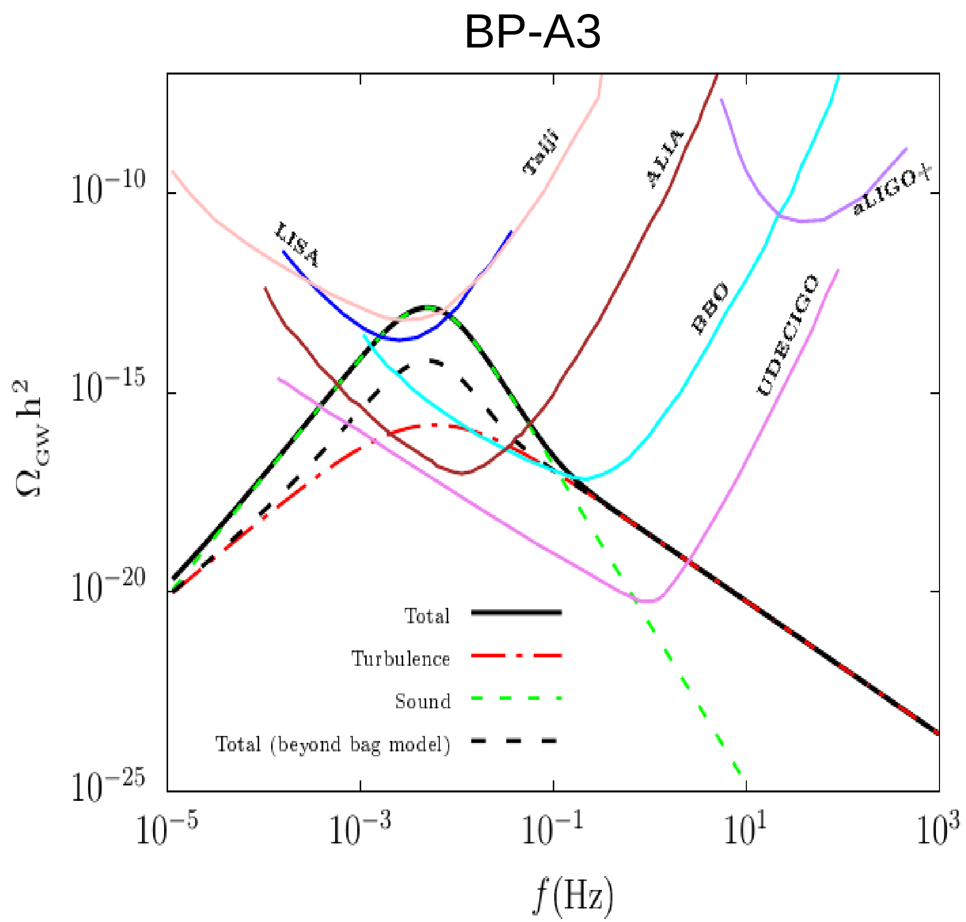

Plots of GW energy density spectrum within and beyond the bag model with respect to frequency

The peak of GW spectrum lies within the sensitivity of various future proposed GW experiments

However, the SNR values are not found to be healthy enough to guarantee a positive detection in LISA and BBO.

Chatterjee, Datta & SR, JHEP06(2022)108

Conclusion

The physics of the EWPT (and hence EWBG) becomes intricately connected to the DM and collider (LHC) phenomenologies.

Due to DM and collider constraints the SFOEWPT favoured parameter space (small $\mu_{\mathrm{e}ff}$) is under tension.

Electroweakino searches at the LHC push $\mu_{\mathrm{e}ff}$ towards larger values.

EWPT could still remain to be of strong, first-order type even for $\mu_{\mathrm{e}ff}$ as large as $\sim$ 425 GeV

Two-step phase transition is a more likely phenomenon at larger $\mu_{\mathrm{e}ff}$

Satisfying all experimental constraints SFOEWPT is still possible in NMSSM

The GW signals resulting from the strong FOPTs in these scenarios could be detected at future dedicated experiments.

It is expected that HL-LHC will test this region of parameter space

Further study required to estimate the baryon asymmetry of the universe in the scenario discussed in this work

Thank You

Back up

Model-independent energy budget of cosmological first-order phase transitions — A sound argument to go beyond the bag model

Felix Giese, Thomas Konstandin and Jorinde van de Vis

DESY,
Notkestraße 85, D-22607 Hamburg, Germany

E-mail: felix.giese@desy.de, thomas.konstandin@desy.de, jorinde.van.de.vis@desy.de

Received May 5, 2020
Accepted June 29, 2020
Published July 27, 2020

Abstract. We study the energy budget of a first-order cosmological phase transition, which is an important factor in the prediction of the resulting gravitational wave spectrum. Formerly, this analysis was based mostly on simplified models as for example the bag equation of state. Here, we present a model-independent approach that is exact up to the temperature dependence of the speed of sound in the broken phase. We find that the only relevant quantities that enter in the hydrodynamic analysis are the speed of sound in the broken phase and a linear combination of the energy and pressure differences between the two phases which we call pseudotrace (normalized to the enthalpy in the broken phase). The pseudotrace quantifies the strength of the phase transition and yields the conventional trace of the energy-momentum tensor for a relativistic plasma (with speed of sound squared of one third).

We study this approach in several realistic models of the phase transition and also provide a code snippet that can be used to determine the efficiency coefficient for a given phase transition strength and speed of sound. It turns out that our approach is accurate to the percent level for moderately strong phase transitions, while former approaches give at best the right order of magnitude.

JCAP07(2020)057